energies

MDPI

Article

Study on Methane Distribution in the Face Zone of the Fully Mechanized Roadway with Overlap Auxiliary Ventilation System

Dariusz Obracaj *, Marek Korzec and Paweł Deszcz

Faculty of Civil Engineering and Resource Management, AGH University of Science and Technology, Mickiewicza 30 Av., 30-059 Kraków, Poland; mkorzec@agh.edu.pl (M.K.); deszcz@agh.edu.pl (P.D.)
* Correspondence: obracaj@agh.edu.pl; Tel.: +48-12-6172180

Abstract: An overlap auxiliary ventilation system is very often used for driving roadways in methane-rich coal seams. An overlap zone between the outlets of the forcing duct ends with a whirl flow air-duct (WFAD) and the exhaust duct ends with a dust scrubber that is created by applying the overlap system. This study examines the distribution of methane concentrations at various distances in the overlap zone. Maintaining a long overlap zone could increase the advance of the face. Therefore, the impact of overlap zone length on the methane concentration distribution, in and beyond the overlap zone, is investigated. The evaluation of methane concentrations is performed utilizing a well-established computational fluid dynamics (CFD) approach. The mathematical model of methane emissions into the roadway is adopted. Moreover, the CFD model is validated. A vortex of the return air, caused by the free airstream flowing out of the dust scrubber, is found. This air vortex is responsible for higher methane concentrations at the end of the overlap zone. Therefore, the conclusion can be drawn that maintaining the length of the overlap zone at 5 m to 10 m should be done to control permissible methane concentrations.

Keywords: mine ventilation; auxiliary ventilation system; forcing with exhaust overlap ventilation system; CFD modelling; methane concentrations; airflow patterns

check for updates

Citation: Obracaj, D.; Korzec, M.; Deszcz, P. Study on Methane Distribution in the Face Zone of the Fully Mechanized Roadway with Overlap Auxiliary Ventilation System. *Energies* **2021**, *14*, 6379. https://doi.org/10.3390/en14196379

Academic Editor: Maxim Tyulenev

Received: 24 August 2021
Accepted: 4 October 2021
Published: 6 October 2021

Publisher's Note: MDPI stays neutral with regard to jurisdictional claims in published maps and institutional affiliations.

Copyright: © 2021 by the authors. Licensee MDPI, Basel, Switzerland. This article is an open access article distributed under the terms and conditions of the Creative Commons Attribution (CC BY) license (https://creativecommons.org/licenses/by/4.0/).

1. Introduction

Appropriate working conditions in mining excavations are ensured using through-flow and auxiliary ventilation systems. There is the risk of dangerous methane concentrations during the advance of development headings in a methane-rich coal seam. Therefore, an effective auxiliary ventilation system is vital. The purpose of using an auxiliary ventilation system during roadway drivage in a methane-rich coal seam is to supply the desired amount of air to the face so that a permissible methane concentration is not exceeded along the entire length of the roadway [1–3].

There are three auxiliary ventilation systems in the driven roadway: force, exhaust and overlap systems. There are two technical solutions among overlap auxiliary ventilation systems. One of them is called a primary forcing with an exhaust overlap system, and the other is called a primary exhaust with a forcing overlap system [1,4–7]. These ventilation systems are selected depending on the technology of roadway drivage and environmental threats, such as methane, coal dust, and thermal conditions, which can result in explosions and/or health issues for miners.

A primary forcing with an exhaust overlap ventilation system is usually used for methane emissions and airborne dust generation from the fully mechanized face of the roadway. Essential components of the system include the primary forcing duct and a short exhaust duct. The advantage of the system is the possibility of dedusting air, taken from the face to the exhaust duct, by including a dust collector. The disadvantages of the system are the zones with various velocities in the cross-section of the roadway and the necessity of constantly moving the exhaust duct, which slows down the advance of the mining

roadway. In practice, the overlap zone of the ducts may be lengthened, which may lead to methane layering and the appearance of dangerous concentrations under the roof of the roadway.

For over three decades, numerical modelling has been used to improve safety in driving roadways in methane-rich coal seams. In addition to ensuring mine safety, it is also essential to reduce energy costs for ventilation purposes. Practical solutions for face zone ventilation are mainly sought to remove the dust generated during mechanical mining of rocks in the face of advanced roadways [8,9], methane emitted from rock masses into the roadway [10], or blasting gases while using explosives [11]. One part of the published research concerns developments that are not equipped with machines and other devices. However, there are also research results that take into account the equipment of a roadway face. For example, the influence of a scrubber in the face zone on the distribution of methane concentrations in advancing faces was investigated by, among others, Wala et al. [12,13] and Petrov et al. [14].

Many studies on the auxiliary ventilation of driven roadways in coal mines show dead zones where higher methane concentrations may form [15–17]. Cao and Liu [10] pointed out that the mean velocity across a tunnel should be kept at 0.5 m/s to maintain a fully developed tube flow to prevent methane build-up under the tunnel roof.

Kurnia et al. [18] presented some studies on methane dispersion in an underground mine tunnel, assuming a constant methane emission rate and constant methane source velocity. The influence of the number and location of emission sources on the distribution of methane concentrations in the tunnel's cross-section with forced ventilation was demonstrated. However, the impact of the machinery and equipment of the tunnel was not taken into account.

Torano et al. [1] published results of a computational fluid dynamics (CFD) simulation of the methane distribution in a roadway with a forcing ventilation system. The k-epsilon turbulence model was selected and verified using field measurements. They indicated three points of air velocity inversion in the tested excavation and showed the variability of methane concentration along a 60-m section from the face of a roadway. In addition, they demonstrated the possibility of identifying zones with an increased methane concentration. Finally, they suggested the option of using CFD simulations to identify zones with increased methane concentration for reinforced ventilation, such as a forcing system with an exhaust overlap.

Sasmito et al. [19] studied the behavior of methane flow at the blind faces of a room-and-pillar underground coal mine to effectively remove methane. They indicated that the Spallart-Almaras turbulence model is helpful for this type of mine excavation due to the low computational time. They analyzed both exhausting and forcing ventilation systems with the use of brattices.

Hasheminasaba et al. [20], using CFD methods, investigated the effect of cooperation of a ventilation brattice with an exhausting duct system on the distribution of methane concentration in a 12-m section of a dead-end, which did not have machines or operating devices. Rahimi et al. [3] presented methane distribution based on the results of CFD analyses from the same analyzed mine excavation. They used a Monte Carlo simulation to determine gas emissions based on the uncertainty of the gas content. As a result, the optimum ventilation air characteristics were found to minimize high costs and provide a safe environment at the working face.

Numerical simulations of more than one gas distribution in roadways or tunnels are rarely considered [2].

The most popular solution for auxiliary ventilation is a primary forcing system with an exhaust overlap, including a whirl flow-air duct (WFAD) installed at the end of the forcing duct. The WFAD ensures a swirling airflow both towards the face and in the overlap zone of air ducts. To the best of the authors' knowledge, the influence of the length of the overlap zone on the distribution of methane concentration released during working at the face has not been investigated. Airflow simulations in a fully mechanized tunnelling face with

similar devices were carried out by Hua et al. [6], using the so-called "multi-radial swirling flow generator" and by Hua et al. [7], employing a multi-radial vortex airflow generator. In general, the impact of the location of generators on the effectiveness of dedusting was examined in these works.

The main objective of auxiliary ventilation with an overlap system is to maintain permissible methane concentrations in both the face and overlap zone. From the point of view of work organization at the face, it would be advisable to minimize scrubber shifting frequency and to simultaneously extend the exhaust duct. As mentioned above, such organizational activities increase the length of the ducts' overlap zones and the appearance of potential methane concentrations. Therefore, the question arises, "what length of the zone should be kept to carry out work safely". A method based on CFD modelling was chosen to solve this issue. The model is developed based on the driven roadway in a coal mine. The results of the measurements obtained from that roadway allow to validate the CFD model.

2. Materials and Methods

2.1. Research Background

The primary forcing with an exhaust overlap system consisted of a forcing duct ending in a WFAD. The secondary exhaust duct was connected to the scrubber and was used to dilute methane and remove dust from the face zone. The inlet to the exhaust duct was located near the face. Air ducts were located partially in parallel, which formed the overlap zone. The WFAD was not located in the overlap zone, and was designed to create swirling air movement towards both the face and the overlap zone.

A duct cassette or storage duct can be placed in front of the WFAD, ending the primary forcing duct. Using the WFAD aimed to remove methane accumulations from under the roof and direct the dust cloud towards the inlet, to the short exhaust duct containing the scrubber. An electrically powered rotor was mounted at the inlet of the whirl-flow air duct. The swirling made the air flow through a 2-cm-wide slot located along the whole whirl-flow air duct. The air velocity was constant along the whole length of the slot. The outlet of the WFAD was closed with a cut-off damper. The opened damper resulted in air outflow towards the face, not through the slot. Such a ventilation option is possible in the case of a non-working face. The WFAD can work on the left and right sides of the roadway without needing to change its structure. The rotor of the WFAD was not a typical fan rotor, and it did not create resistance to the airflow along the forcing duct. When the rotor was switched off, the appropriate structure of the rotor caused it to stop after about 20 s while maintaining the same airflow rate from the forcing duct.

Figure 1 shows the principle of operation of such an auxiliary ventilation in a roadway face as well as the WFAD. More detailed information on the WFAD and the dedusting equipment can be obtained from the authors.

In Polish mines, the face zone's required air quantity should be no lower than the mean velocity of 0.3 m/s in the roadway, except for the overlap zone. However, at least 20% of the airflow in the exhaust duct of the scrubber must flow into that zone.

Currently, it is believed the overlap zone should not be longer than 10 m. These recommendations are based on the belief that a more extended zone may increase methane concentrations under the roof due to lower air velocities. However, this concept has not been confirmed on site.

Maintaining a predetermined distance of the overlap zone requires, in turn, a frequency shift of the scrubber together with the advancing face. From the perspective of work organization at the face, it would be advisable to minimize the frequency of shifting and, at the same time, extend the forcing duct ending in the WFAD. If the scrubber is immobilized for a longer time, the distance between the face and the exhaust duct will increase together as the face advances. This can be remedied by adding another exhaust duct; thus maintaining a constant distance between the duct inlet and the face. However, the overlap zone of the systems will then lengthen.

The heuristic approaches of researchers have determined the effectiveness of the overlap system with a WFAD so far; however, no one has thoroughly investigated the gas concentration fields of such a ventilation system for an advancing face of a roadway. The question arises as to how the increase in the length of an overlap zone affects the distribution of methane concentrations within it. In response to this, a numerical model was built to simulate the field of both velocity and methane concentrations, considering the dimensions and equipment of a particular roadway.

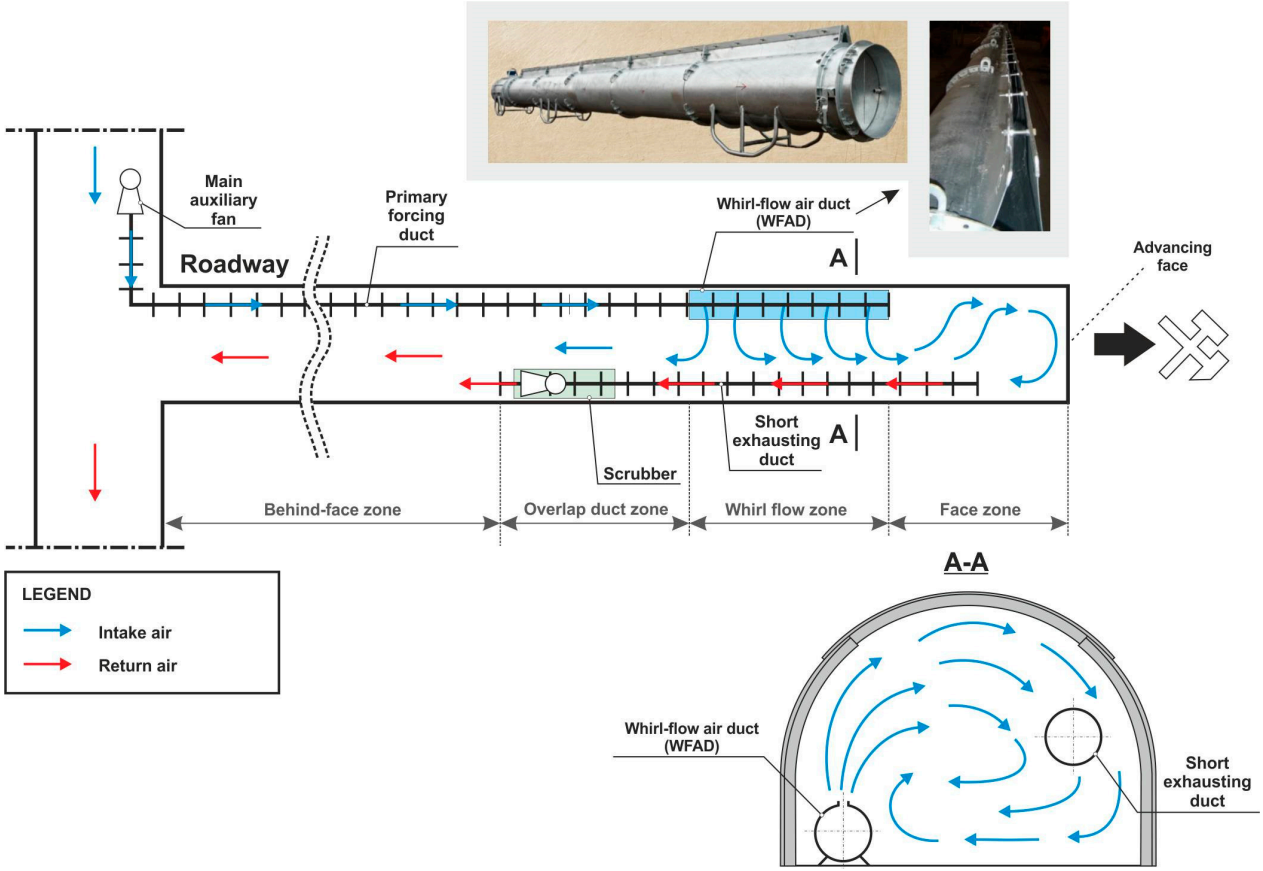

Figure 1. Layout of the primary forcing with exhaust overlap ventilation system.

2.2. Geometric Model

The analyzed Belt Roadway was driven in one of coal mines, at a depth of 950 m, in the Upper Silesia Coal Basin (USCB), Poland. The roadway was run, among other things, in a 1.0-m thick coal seam 405/1, which was predicted to release 5.0 m^3/min of methane. The total target length of the roadway driven was 1400 m. The roadway was driven with a 5 per mile slope. The roadway, with an arched section of 17.6 m^2, was supported with arch support V36/12/4 yielding steel sets. The spacing between the yielding sets was 0.8 m. The cross and longitudinal sections of the 100-m distance to the face are presented in Figure 2. The average advance rate of the roadway driven by an Alpine AM-75 reached 8 m per day.

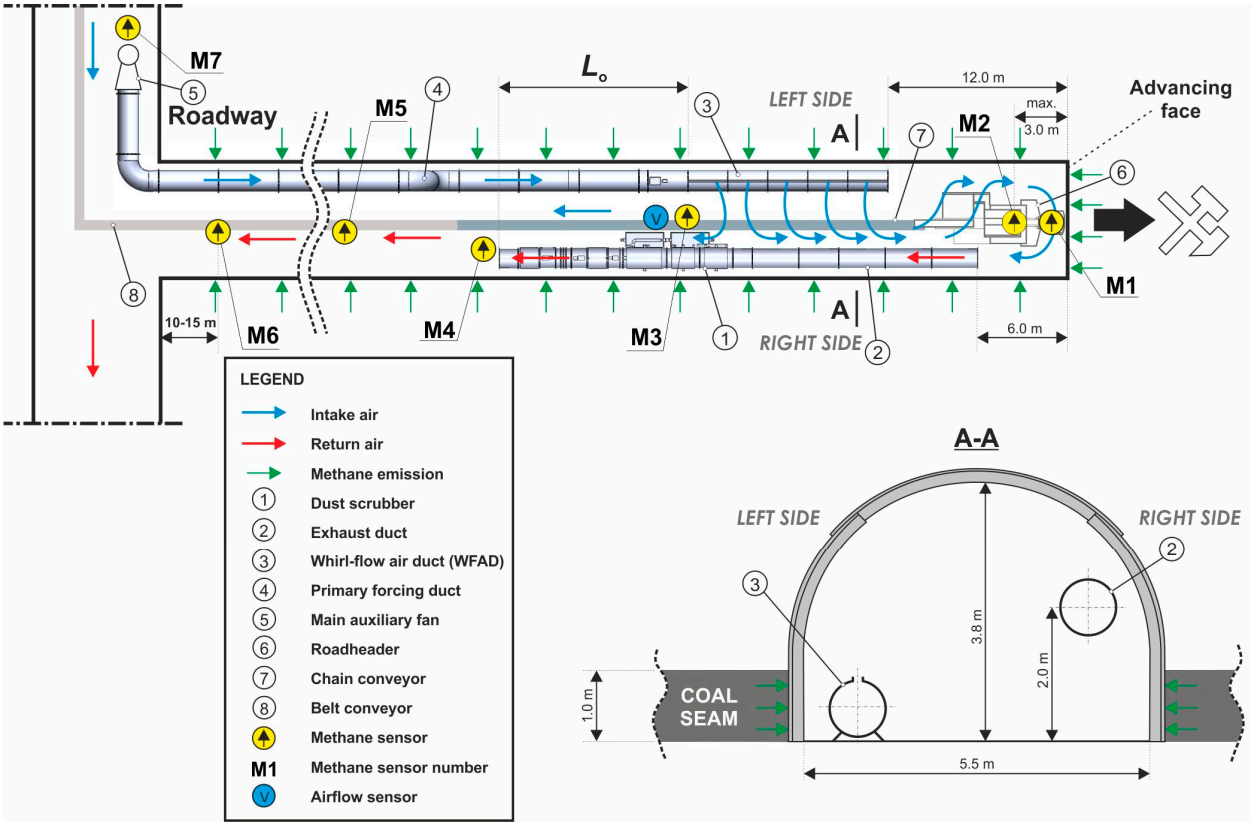

Figure 2. Scheme of equipment in the analyzed Belt Roadway.

Analysis of methane distribution in the roadway required a precise determination of the devices used; namely, the ventilation devices, mining machines, and conveyors. The following devices were used in this case:

- road header machine, AM75;
- whirl-flow air duct, WIR-1000 (WFAD);
- dust collector, UO 800-1000;
- belt conveyor, GWAREK-1000;
- chain conveyor, SKAT 80/KJ.

The equipment was located centrally in the cross-section of the roadway. Furthermore, ventilation devices were located at the roadway walls, following the rules of the overlap ventilation system. The scrubber was suspended 6 m from the face, and its axis was 2 m above the floor. The WFAD was located on the floor at a distance of 12 m from the face.

2.3. Analyzed Cases

In practice, it is easier to lengthen both the primary forcing duct and the exhaust duct during roadway driving than to move the scrubber behind the advancing face of the roadway. However, this results in lengthening the overlap zone, as such, there is a possibility of increased methane concentrations along the overlap zone. Therefore, four cases of different lengths of overlap zones were considered: 5, 10, 15, and 20 m, respectively. The assumptions for the CFD calculations are presented in Table 1.

Table 1. Assumptions for CFD calculations.

Case (According to Figure 2)	Airflow Rate, kg/s	
	WFAD	Dust Scrubber
L_o = 5 m	8	6.64
L_o = 10 m		6.61
L_o = 15 m		6.67
L_o = 20 m		6.65

The model takes into consideration well-established sources of steady and homogeneous methane emissions with the assumption of the continuous roadheader operation.

3. Numerical Methodology

3.1. Model Development

Preparation of the computational model required making a fluid domain based on the physical model of the roadway. In this model, considering one of the flow conditions, two fluid domains were made without voids, but sharing the same topology. This allowed to improve the quality of the computational mesh, limit its elements, and thus reduce the computation time. The first fluid object was extracted by cutting out a fragment of the devices in each roadway cross-section. Then, the second fluid object was inserted as a separate object into the place of the scrubber cut-out.

The numerical model, based on computational fluid mechanics, was performed using ANSYS Workbench version 19.3. The geometric model of the roadway was developed in SolidWorks 2018 and was adapted for simulation in Ansys Space Claim. The actual dimensions of the part of the roadway were applied to build the spatial geometry. The analysis consists of four numerical models varying in exhaust duct length, ending in the scrubber.

Figure 3 presents the location of the equipment in the face zone of the model.

(**a**)

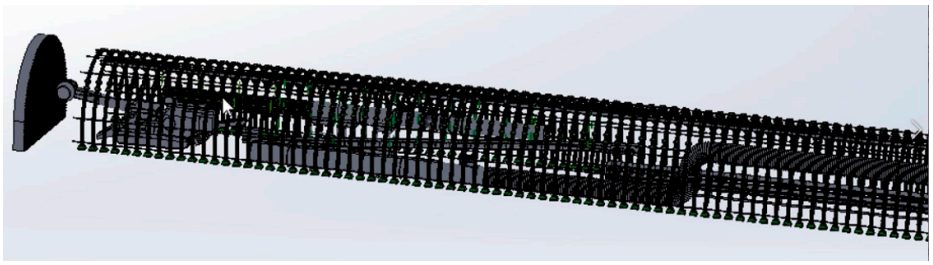

(**b**)

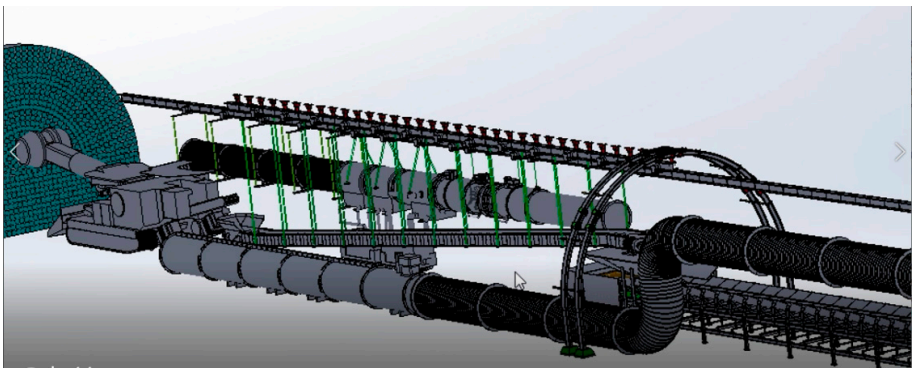

Figure 3. The arrangement of excavation devices in the geometrical model (5-m overlap zone), (**a**) full view, (**b**) view without arch support.

3.2. Discretization of the Geometrical Model

The same meshing software was used in simulations for all cases with the same settings. Fluent Mesher was applied to create the computational mesh instead of the Ansys Mesher Module; it was used to get a better-quality mesh.

The convergence test for the computing mesh was conducted for a few cases. Total computing time (from 22 h to 112 h), net balance of the flow (from -0.0000314 kg·s^{-1} to -0.0000076 kg·s^{-1}), number of elements (from 6.5 million to 29 million), single iteration computing time, and the quality of the mesh (from 0.42 to 0.43), were checked in the test, respectively.

Three different meshes were made in this analysis for one case (that of the 5 m overlapping zone). It was assumed that the mesh size increased twice between tested cases. Three models with meshes of 6.5 million elements, 14 million elements, and 29 million elements were obtained. The net flow balance in the computing models, between the inlets and outlets, was conducted for the airflow without methane.

The Watertight scenario discretized the prepared geometry. All four computational models were digitized using the same mesher, with the same settings for each case. The size of the mesh for objects in the geometry was determined in the first stage, as follows:

- dust scrubber, 0.175 m;
- slot in the whirl-flow air duct, 0.0035 m;
- ducting, 0.175 m;
- all walls on the perimeter of the roadway, 0.2 m;
- belt conveyor, 0.125 m.

When the local sizing mesh was completed, the mesh size was varied from 0.0035 m to 0.35 m. The surface mesh was made in the whole numerical domain using settings presented in Table 2.

Table 2. Features used in preparation of surface mesh.

Feature	Constant/Setup
Growth rate	1.2
Size functions	Curvature and proximity
Curvature normal angle	15°
Cell per gap	3
Scope proximity	Faces and edges
Smooth folded faces	15
Invoke zone separations	Auto angle
Separation angle	30°
Auto zone types	Yes
Quality improve skewness	0.2
Quality improve max angle	90°

However, the generated surface mesh was of low quality, which influenced the quality of the volumetric mesh; therefore, its quality was improved using algorithms upgrading the surface mesh, according to the following settings:

- quality improvement of max angle: 0.85;
- quality improvement of iterations: 500;
- quality improvement of collapse skewness limit: 0.85.

As a result, surface meshes with a maximum skewness of 0.62 ± 0.2 for all cases were obtained. In the following step, the geometries were determined, i.e., their physical features, boundary conditions, external interfaces, and fluid regions. Then, volume discretization of the computational domain was performed usig the parameters presented in Table 3.

Table 3. Features used in preparation of surface mesh.

Feature	Constant/Setup
Offset method	Smooth transition
Number of layers	5
Transition ratio	0.272
Growth rate	1.2
Ignore inflation at acute angles	Yes
Inflation gap factor	0.1
Inflation max aspect ratio	25
Inflation mix aspect ratio	1
Keep first inflation layer height	Yes
Adjacent attach angle	45°
Fill	Poly-hexcore
Peel layers	1
Max cell length	0.25 m
Invoke persistent renaming	No
Use size field	No
Polyhedral mesh feature angle	30°
Avoid 1/8 octree transition	Yes
Fill polyhedral in solid	No

The obtained computational mesh was still of low quality; therefore, the re-algorithms were used to improve the quality of the computational mesh, this time for the volumetric mesh, with the following settings:

- Cell quality limit: 0.5;
- Quality improvement of min angle: 15;
- Quality improvement of iterations: 15.

The view of the mesh of an exemplary cross-section is shown in Figure 4. Table 4 shows the obtained results for the parameters of the volumetric computational grids.

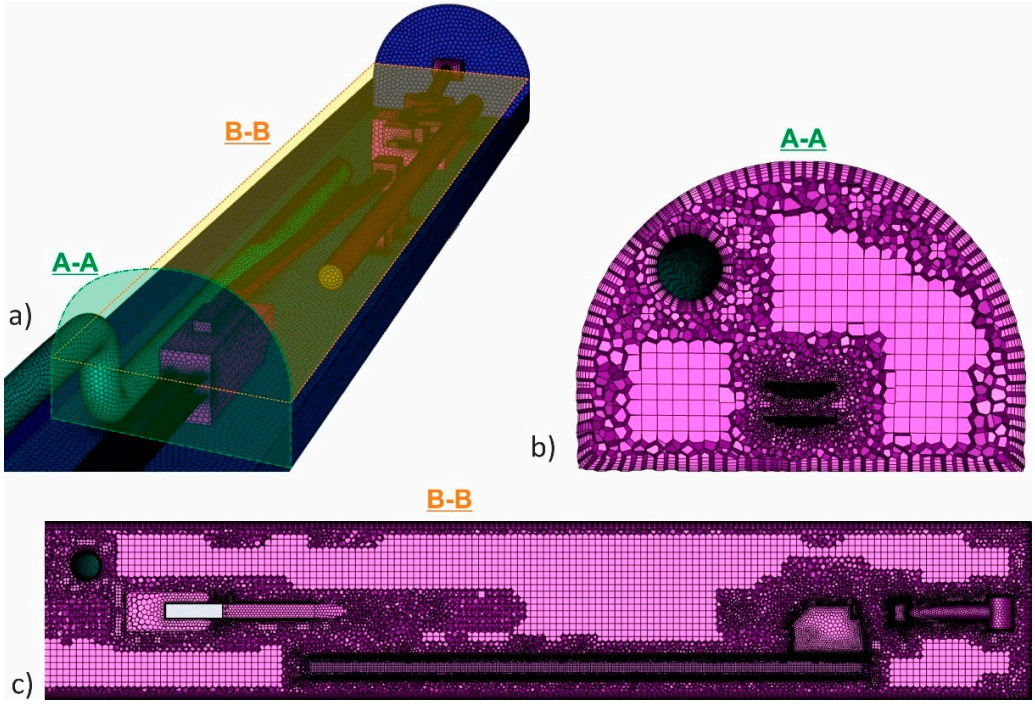

Figure 4. Example of mesh (5-m overlap zone), (**a**) surface mesh, (**b**) volume mesh—cross section, (**c**) volume mesh—longitudinal section.

Table 4. Number of elements and minimal orthogonal quality for each case.

Case	Number of Elements for Excavation	Number of Elements for Dust Collector	Minimal Value of Orthogonal Quality
L_o = 5 m	6,741,976	56,321	0.42
L_o = 10 m	6,524,191	62,063	0.42
L_o = 15 m	6,534,020	72,077	0.43
L_o = 20 m	6,562,580	78,514	0.43

3.3. Sources of Methane Emission

With the advancing faces of mine roadways, methane is emitted from many sources, including exposed planes of the coal seam and mined coal. The total volumetric emission of methane, Q_t, to the roadway was the sum of methane emissions from coal mined, Q_c, from the coal surface in roadway walls, Q_w, and from the exposed coal face, Q_f.

3.3.1. Methane Release from Freshly Mined Coal Transported by a Conveyor

Determined in the laboratory, the methane content of coal, V_i in the developed coal seam 405/1 was 7.7 m^3/t^{daf}. The initial methane content, V_i is the sum of desorbable V_d and residual V_r gas contents. Desorbable gas content was 6.2 m^3/t^{daf}. The change in the desorbable gas content of coal with time, τ, can be expressed by a differential equation:

$$\frac{dV(\tau)}{d\tau} = -c_d \cdot V_d \cdot \tau \quad (1)$$

where $V(\tau)$ is the methane content of desorbed methane remaining in one ton of mined coal after time τ (instantaneous methane content of coal), m^3/t, V_d is the initial value of desorbable gas content. The constant characterizing the rate of methane desorption from the mined coal was determined by c_d, 1/min. The constant c_d depends on the properties of the carbon–methane phase system, i.e., mainly the fragmentation of coal and the size of the developed area, temperature, and pressure of the adsorbed gas, τ is the time counted from the beginning of methane separation from the mined coal, min.

The solution to Equation (1) was given in [21,22]. Assuming the initial condition in the form: $\tau = 0$ and $V(\tau) = V_d$, the solution of Equation (1) is obtained as follows:

$$V(\tau) = V_d \cdot \left(1 + e^{-c_d \cdot \tau}\right) \quad (2)$$

Assuming the continuous operation of both the roadheader and the conveyor, amount of methane Q_c, m^3/min, which is released from the mined coal for time τ can be presented as follows:

$$Q_{c(x)} = A \cdot V_d \cdot \left(1 - e^{-\frac{c_d \cdot x}{v_t}}\right) \quad (3)$$

where v_t is the transport speed of the output, m/min, x is the coordinate of the length measured along the axis of the roadway from the coal loading site, m and A is the continuous coal output from the face, t/min.

Constant c_d ranges from 1.4 to 1.6 1/min for the Upper Silesian Coal Basin [23].

3.3.2. Methane Release from Coal Surfaces along Walls of Roadway

The rate of gas emission change from the exposed coal surface of roadway walls, q_w $m^3/(m^2$ min), can be determined as follows [24]:

$$q_w = Q_o \cdot e^{-k \cdot \tau} \quad (4)$$

where Q_o is the initial methane emission at the time of exposure of the coal surface, $m^3/(m^2$ min), k is the constant characterizing the rate of methane emission from exposed coal surface, 1/min, which depends on the rate of methane desorption from coal but also

the permeability of the fracture zone around the driven roadway [25], τ is the time that has passed since the exposure of the coal surface, min.

Constant k assumes values in the range of 0.0001–0.0002 1/min [21]. By assuming a constant face advance, the following expression is used to determine the volumetric flow rate of methane from two surfaces of coal, located on the left and right of the roadway [24]:

$$Q_{w(x)} = \frac{2 \cdot m \cdot Q_o \cdot v_d}{k \cdot \left(1 - e^{-\frac{k \cdot x}{v_d}}\right)} \quad (5)$$

where m is the thickness of the exposed coal seam, m, v_d is the advance of the roadway face, m/min.

Methane emission at the moment of exposing the coal surface, Q_o, is the function of initial methane content, V_i [26], and is given as follows:

$$Q_o = 0.0006 \cdot e^{0.25 \cdot V_i} \quad (6)$$

3.3.3. Methane Release from Exposed Coal Surface in Roadway Face

Methane emission from the surface of the roadway face, Q_f at the time of its exposure can be calculated according to formula:

$$Q_f = Q_o \cdot m \cdot b \quad (7)$$

where b is the width of the roadway, m.

Methane emission from the face is a relatively small value.

Table 5 shows the data results for determining methane emission sources that were included in the numerical model.

Table 5. Methane emission sources for numerical modelling.

Parameter	Value	Unit
A	0.035	t/min
v_t	55	m/min
v_d	0.011	m/min
c_d	1.5	1/min
k	0.00015	1/min
V_i	7.7	m^3/t
V_d	6.3	m^3/t
Q_o	0.00443	$m^3/(m^2\ min)$
m	1	m
b	5.5	m

The methane emission model was implemented in the CFD simulation model. Several conditions for maintaining the flow and dispersion of methane for four cases of the length of the overlap zones were investigated to obtain an answer to the influence of increasing the overlap distance on the distribution of methane concentrations and safety of mining works.

3.4. Boundary Conditions and Solver

A Fluent solver was used to perform numerical calculations. The simulation was performed as a stationary one, taking gravity into account. The following data were selected in the settings of the computational model:

- k-e Realizable flow model with enhancement wall treatment function;
- model species for the methane-air mixture (components: methane, air) with the density model set to volume-weighted mixing law;

- energy equation was excluded due to the change in the method of calculating the density of gas mixture as the isothermal condition was assumed.

The model was prepared in the form of two volumes sharing the same topology. This assumption permitted for using the following conditions for cell zones:

- For the first zone—the roadway—two sources were added. The first one relates to methane emission to the roadway, while the second one results from the emission source, i.e., the source of mass. The model of methane emission presented in Section 3.3 was implemented using the User Defined Function, prepared especially for this case. Its task is to ensure the optimal emission along the whole length of the excavation from selected surfaces. The UDF overlays the first discretization layer because there is only methane in each iteration (boundary condition). This function is used for methane emission from the walls, the face, and the upper surfaces of the belt and scraper conveyors. The total value for the selected areas is expressed by:

$$f(Q_{CH_4}) = \begin{cases} 0.05\frac{kg}{s} \text{ for coal surface in the face,} & 0.025\ \frac{kg}{s} \text{ for } x \leq 6, \text{ and} \\ 0.0164 \cdot e^{-0.012 \cdot (x-6)} \text{ for } x > 6 \end{cases} \quad (8)$$

where x is the distance of the unit surface from the face of the roadway and depends on the distance of a given mesh from the face and is proportional to the size of the mesh itself.

- For the second zone—the dust scrubber—the source of momentum towards axis Z of value 9 N/m^3 is related to the flow rate in the scrubber of value 6.64 $m^3/s \pm 0.03\ m^3/s$.

The boundary conditions were defined as a mass-flow-inlet for the WFAD of 8 kg/s in the normal direction to the slot of the WFAD. The pressure-outlet condition for this slot was left as the default value.

3.5. Governing Equations

The k-ε model of turbulence for the mixing law of the mixture of methane-air without additional factors was used for considering the roadway model. Many factors affect the motion of methane, and airflow's carrying effect is the most significant. The simulation results of the airflow field determine the accuracy of the methane motion calculation. The mathematical model of the airflow movement in a fully-mechanized roadway face was accurately established using ANSYS Fluent software [27]. The equation for the conservation of mass, or continuity equation, can be expressed as:

$$\frac{\partial \rho}{\partial t} + \nabla \cdot \left(\rho \vec{v}\right) = S_m \quad (9)$$

Equation (9) is the most common form of the mass conservation equation, and it is applicable to compressible and incompressible fluids. Source S_m is the mass added to the continuous phase from other dispersed phases or any user-defined source (UDS).

The momentum equation of airflow can be expressed as follows:

$$\frac{\partial}{\partial t}\left(\rho \vec{v}\right) + \nabla \cdot \left(\rho \vec{v} \vec{v}\right) = -\nabla p + \nabla \cdot \left(\overline{\overline{\tau}}\right) + \rho \vec{g} + \vec{F} \quad (10)$$

where p is the static pressure, $\overline{\overline{\tau}}$ is the stress tensor, $\rho \vec{g}$ and $\vec{F}$ are the gravitational body force and external body force, respectively. $\vec{F}$ contains other model-dependent source terms.

Stress tensor $\overline{\overline{\tau}}$ can be expressed as follows:

$$\overline{\overline{\tau}} = \mu\left[\left(\nabla \vec{v} + \nabla \overrightarrow{v^T}\right) - \frac{2}{3}\nabla \cdot \vec{v} l\right] \quad (11)$$

where μ is the molecular viscosity, l is the unit tensor and the second term on the right-hand side of the formula is volume dilatation.

The turbulence kinetic energy and rate of dissipation are obtained as follows:

$$\frac{\partial}{\partial t}(\rho k) + \frac{\partial}{\partial x_j}(\rho k U_j) = \frac{\partial}{\partial x_j}\left[\left(\mu + \frac{\mu_t}{\sigma_k}\right)\frac{\partial k}{\partial x_j} \right] + G_k + G_b - \rho\varepsilon - Y_M + S_k \quad (12)$$

$$\frac{\partial}{\partial t}(\rho \varepsilon) + \frac{\partial}{\partial x_j}(\rho \varepsilon U_j) = \frac{\partial}{\partial x_j}\left[\left(\mu + \frac{\mu_t}{\sigma_\varepsilon}\right)\frac{\partial \varepsilon}{\partial x_j} \right] + \rho C_1 S\varepsilon - \rho C_2 \frac{\varepsilon^2}{k + \sqrt{v\varepsilon}} C_{3\varepsilon} G_b + S_\varepsilon \quad (13)$$

$$C_1 = \max\left[0.43, \frac{\eta}{\eta + 5}\right]; \eta = S\frac{k}{\varepsilon}; S = \sqrt{2S_{ij}S_{ij}} \quad (14)$$

where G_k represents the generation of turbulence kinetic energy due to mean velocity gradients, G_b is the generation of turbulence kinetic energy due to buoyancy, Y_M represents the contribution of the fluctuating dilatation incompressible turbulence to the overall dissipation rate, C_2 and $C_{3\varepsilon}$ are constants, σ_k and σ_ε are the turbulent Prandtl numbers for k and ε, respectively, S_k and S_ε, are user-defined source terms.

4. Validation of Turbulence Model

The filed measurements were made during the Belt Roadway drilling. The length of the overlap zone was kept at 10 m. The measurements were carried out during the first working shift from 6:00 a.m. to 2:00 p.m. They included manual methane concentration measurements using a Drager X-AM 7000 methane meter with 2.5% accuracy of the measured value. Measurements were taken at selected points of the roadway cross-section at the height of 1.0 m and 2.0 m above the roadway floor. Regardless of the manual measurements, the methane concentration data from sensors of the real-time monitoring system in the roadway were obtained. The accuracy of methane monitor sensors was also 0.1% vol. Three typical cross-sections of the roadway with built-in methane sensors were selected to validate the model. The methane sensors were located at a distance of 0.1 m from the roof of the roadway. Selected sensors in the cross-sections are marked in Figure 2. The measurement points in the cross-sections are shown in Figures 5–7, which present the distribution of methane concentrations obtained from the CFD simulation.

- location of the M3 methane sensor at a distance of 22 m to the face (in the overlap zone—2 m from the beginning of the WFAD)—Figure 5,
- location of the M4 methane sensor at a distance of 32 m to the face (at the scrubber outlet)—Figure 6,
- location of the M5 methane sensor at a distance of 42 m to the face (10 m behind the overlap zone)—Figure 7.

Manual measurements were performed three times during roadheader working. Results presented in Figures 5–7 have average values obtained from the measurements mentioned above.

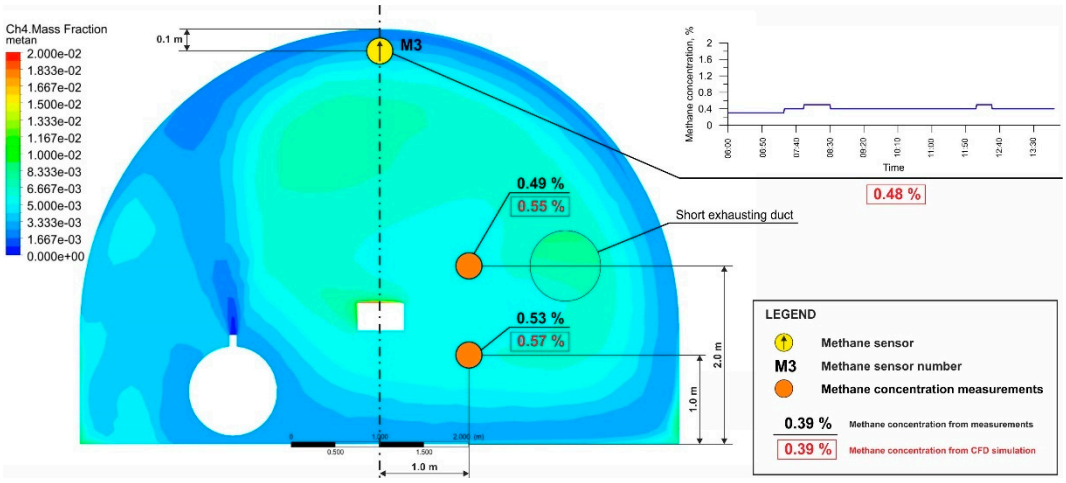

Figure 5. Distribution of methane concentration in the roadway's section at a distance of 22 m from face and the location of the M3 methane sensor (cross-section at a setback distance of 2 m from the whirl-flow air duct).

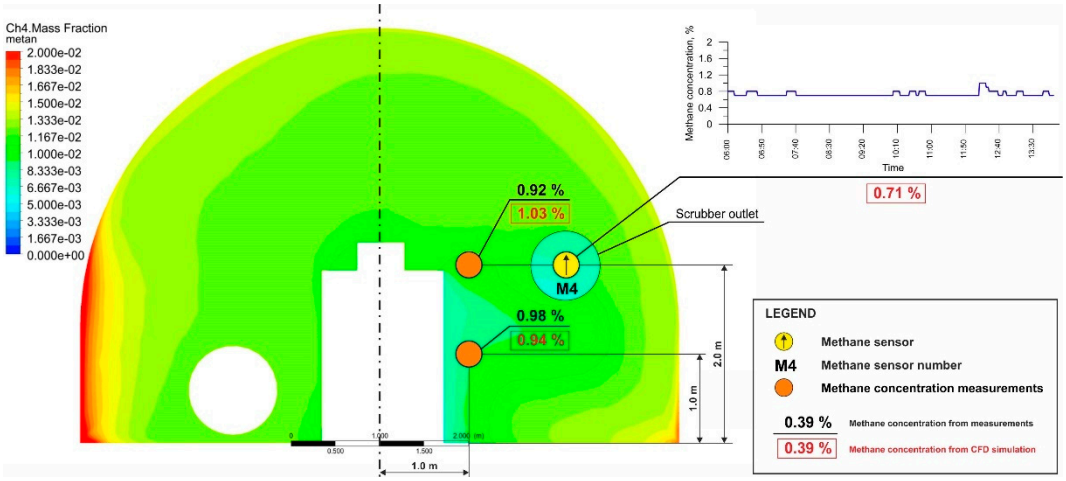

Figure 6. Distribution of methane concentration in the section of the roadway at a distance of 32 m from face with the location of the M4 methane sensor (at the scrubber outlet).

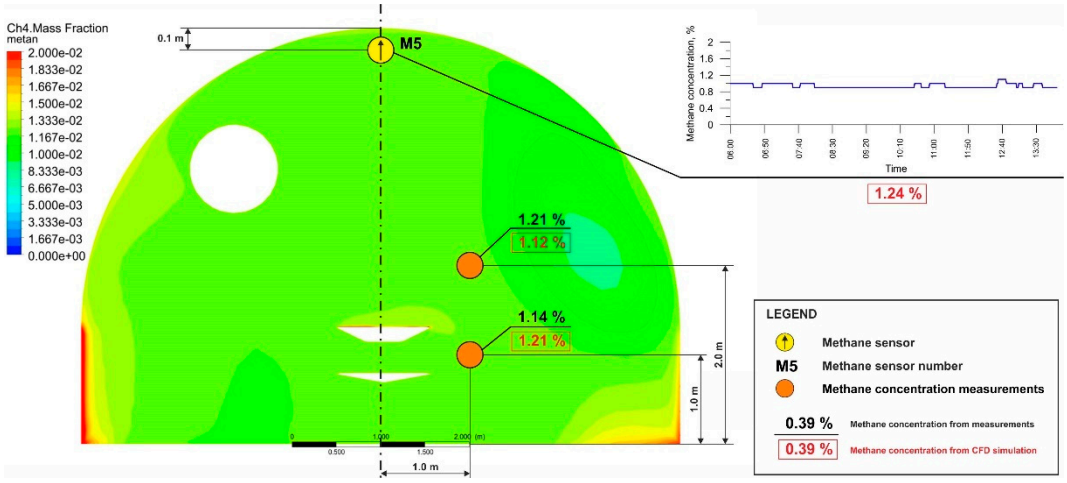

Figure 7. Distribution of methane concentration in the section of the roadway at a distance of 42 m from face with the location of the M5 methane sensor (10 m from the end of the overlap zone).

The airflow rate at the exit of the roadway was also measured. The absolute methane emission into the roadway was calculated based on the determined airflow rate and indications of methane concentration of the M6 sensor. The methane emission ranged from 4.85 m^3/min to 5.15 m^3/min with an average value of 5.00 m^3/min.

The comparison of methane concentrations is presented in Figures 5–7. The difference between the results of measurements and calculations does not generally exceed 10%; therefore, it is assumed that the validation of the adopted turbulence model is approved.

As the behavior of overall airflow and methane concentration for design purposes is investigated, model k-ε realizable with functional enhancement wall treatment was considered to be sufficient.

5. Results and Discussion

The boundary conditions are the same for all four analyzed cases. A total of 80% of the fresh air flowing out of the WFAD moved toward the face, ensuring methane dilution and proper transport of return air to the scrubber. A total of 20% of the fresh air flowed through the overlap zone in a swirling motion.

The only difference that affects the flow of fluids in the roadway is the overlap zone's length. The simulation results indicate that some of the air leaving the scrubber returns along the opposite scrubber's sidewall to the overlap zone. This effect of the vortex crating air backflow has not been detected so far, although previously Li et al. [28] described a similar backflow, but in the face zone when using the forcing ventilation system.

The air vortex is visible at the roadway's left sidewall in Figure 8a,b, for the overlap zones *Lo* = 5 m and L_o = 10 m, respectively. The air entrainment of a free jet flowing out of the scrubber creates the vortex and thus backflow to the overlap zone along the left wall. In turn, Figure 8c,d shows two air vortices at 30 m distance from the scrubber outlet for the cases of L_o = 15 m and L_o = 20 m, respectively.

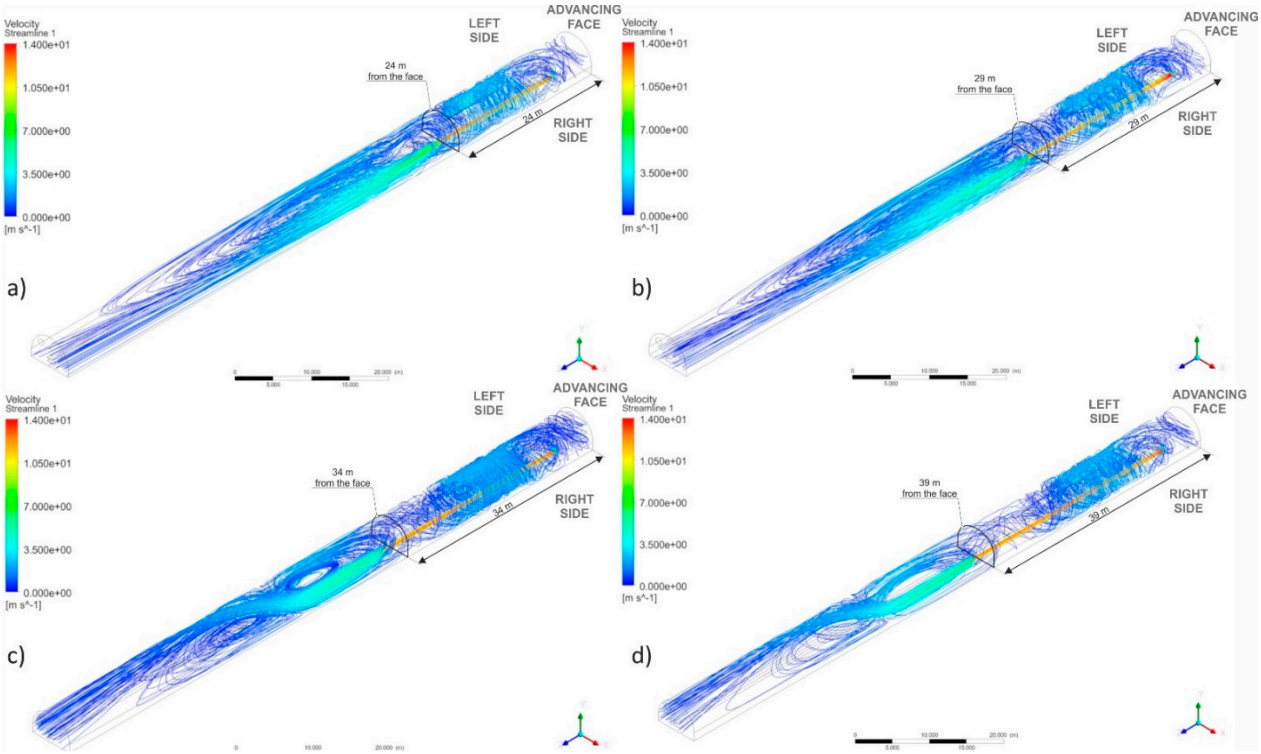

Figure 8. Velocity streamlines (**a**) L_0 = 5 m, (**b**) L_0 = 10 m, (**c**) L_0 = 15 m, (**d**) L_0 = 20 m.

For the cases L_o = 5 m and L_o = 10 m, respectively, the air vortex reaches the swirling airflow zone produced by the WFAD. It collides with the swirling flow downstream of the

whirl-flow air duct. In case L_o = 5 m (Figure 8a), the vortex may disturb the swirl concept of fresh airflow.

On the other hand, for L_o = 15 m and L_o = 20 m cases, a much shorter range of air backflow to the overlap zone is visible than for the cases L_o = 5 m and L_o = 10 m. This is because the collision of the backflow vortex with fresh air occurs at the end of the overlap zone.

The excavation equipment also influences the range of air backflow effects, which is confirmed by the results of other studies [29,30]. Therefore, it is essential to consider equipment in the roadway during numerical modelling, especially with such a complex ventilation as in overlap auxiliary ventilation systems.

The observed phenomena of airflow in such a ventilation system significantly affect the distribution of methane concentration. Figure 9a–d shows that methane concentrations are highest in the face zone, which results from the location and intensity of methane emission sources. A decrease in gas concentration is noticeable in the overlap zone compared to the one in the face zone. In the case of L_o = 5 m, the vortex of air flowing along the left sidewall achieved the WFAD disturb the swirl profile of air flowing out (Figures 8a and 9a).

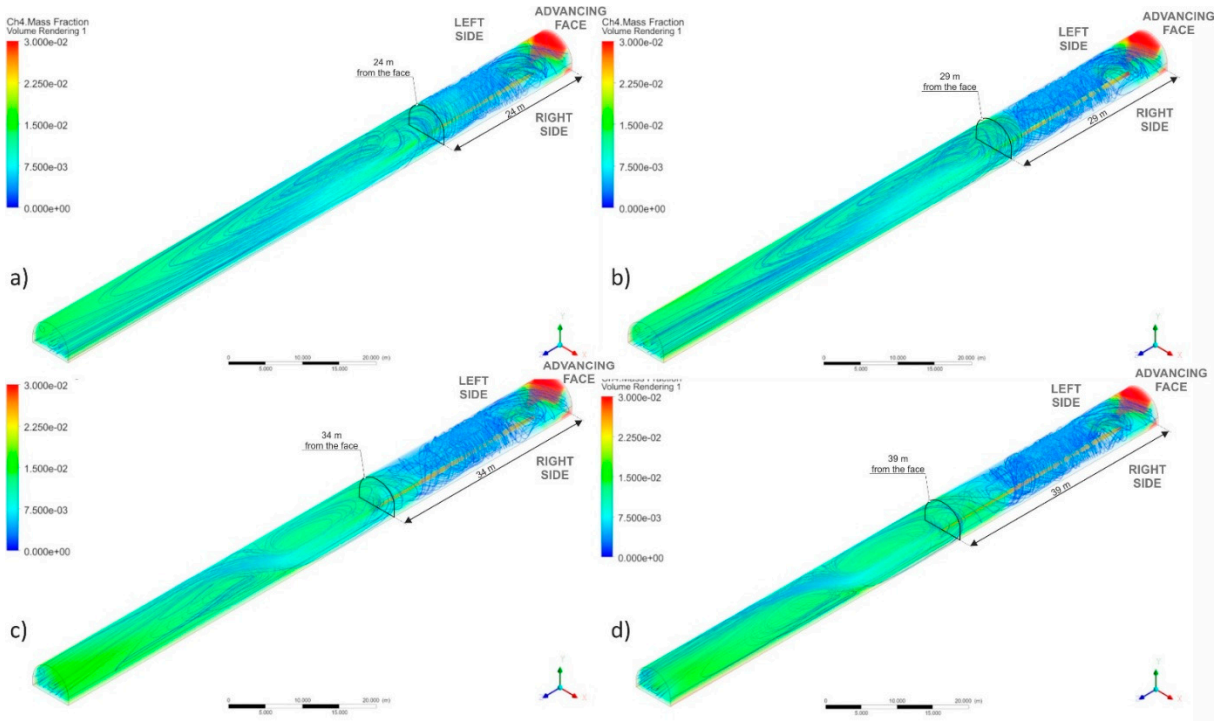

Figure 9. Methane concentration and velocity streamlines—general view, (**a**) L_o = 5 m, (**b**), L_o = 10 m, (**c**), L_o = 15 m, (**d**) L_o = 20 m.

The alignment of the methane concentration concerning the behind-face zone is visible at the end of the overlap zone. The length of the overlap zone influences the profile of the backflow vortex when mixed with the swirling flow of fresh air. As the overlap zone's length increases, the air backflow has more space to spread (Figure 10b–d).

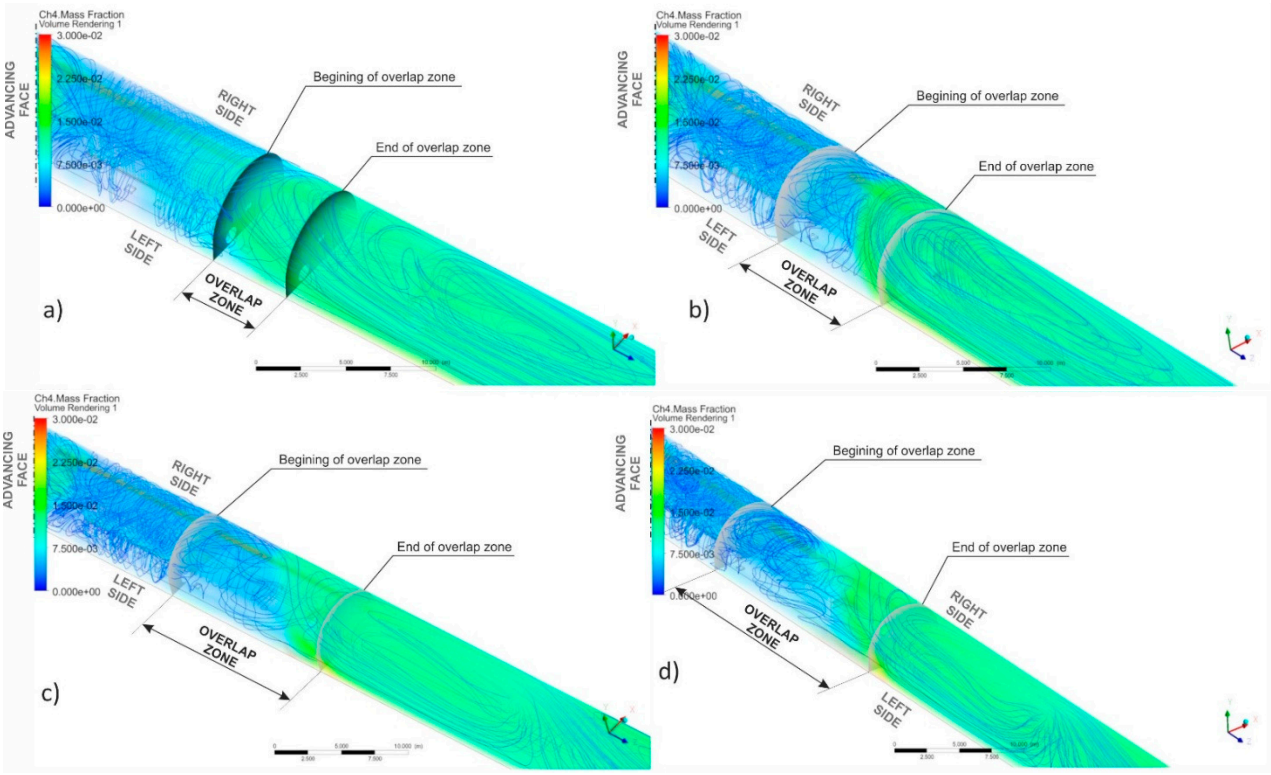

Figure 10. Methane concentration and velocity streamlines in overlap zone, (**a**) L_o = 5 m, (**b**), L_o = 10 m, (**c**), L_o = 15 m, (**d**) L_o = 20 m.

For the case of L_o = 5 m, the vortex flows, even up to 24 m from the face, i.e., 2 m from the beginning of the overlap zone (Figure 10a). The uniform methane concentration in that cross-section is visible (Figure 11a), with a value close to the average methane concentration in the other part of the roadway. This results from the inflow of vortex of return air with an increased methane content. Figure 11b shows the velocity profile at the distance of 10 m from the scrubber outlet. The increase in velocity is visible on the left side of the roadway, delivering air into the overlap zone.

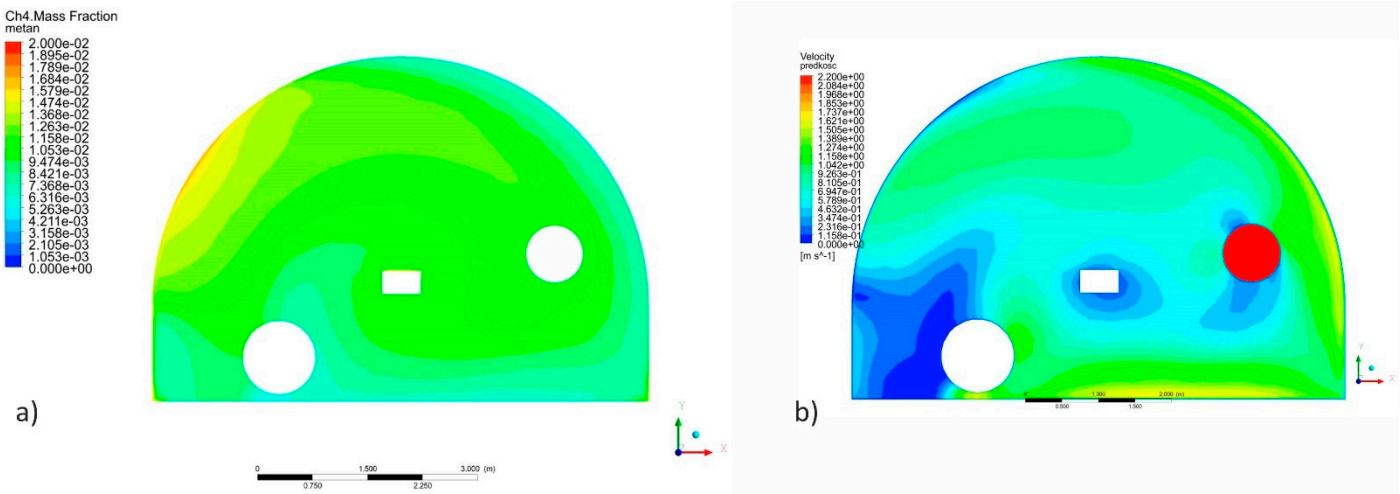

Figure 11. Cross-section of roadway at the distance of 24 m to the face for case L_o = 5 m, (**a**) methane concentration field, (**b**) air velocity field.

For the case of L_o = 10 m, the effect of mixing the vortex with the swirling flow of fresh air appears at the distance of 29 m to the face, i.e., precisely 5 m further than in the case of

L_o = 5 m. Moreover, in this case, the methane concentration was leveled in the cross-section of the roadway (Figure 12a). The effect of turbulence on the airflow velocity is visible at the distance of 7 m to the face, i.e., 29 m from the beginning of the overlap zone (Figure 12b).

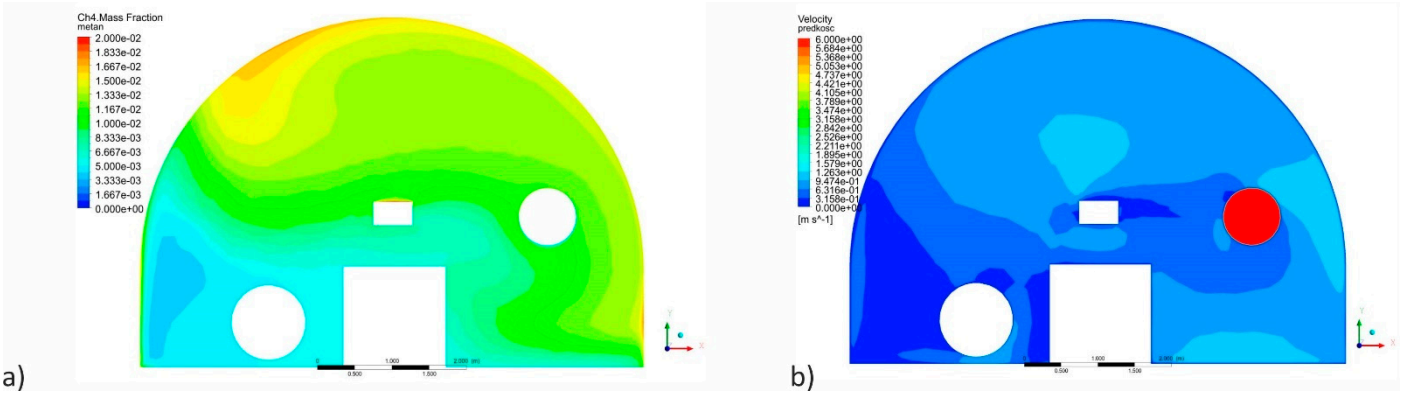

Figure 12. Cross-section of roadway at the distance of 29 m to the face for the case L_o = 10 m, (**a**) methane concentration field, (**b**) air velocity field.

For the cases, L_o = 15 m and L_o = 20 m, the airflow profiles are different from the first two cases because there are two formed air backflow zones that occur in the behind-face zone. These backflows reduce the air velocity in the overlap zone to 0.3 m/s because the air vortex does not flow into that zone due to the formation of the second backflow zone in the behind-face zone on the left sidewall (Figure 9c,d). The free air jet flowing out of the scrubber expands, decreases its velocity to 3.5 m/s and turns towards the left sidewall due to the formation of the reduced pressure zone there. This kind of flow influences the formation of the smaller vortex in the second backflow zone, which is located at the right sidewall of the behind-face zone. The second air vortex has a counter-rotating direction of the air movement compared to the first one. It results in less turbulence under the right sidewall at the overlap zone's edge.

For case L_o = 15 m, the first vortex resulting from mixing the fresh and return air is visible at the distance of 12 m from the beginning of the overlap zone (Figure 10c). Figures 13a and 14a show the methane concentration field with higher values than for L_o = 5 m and L_o = 10 m. Moreover, the air velocities on the left side of the roadway (Figures 13b and 14b) are higher than in the previous cases.

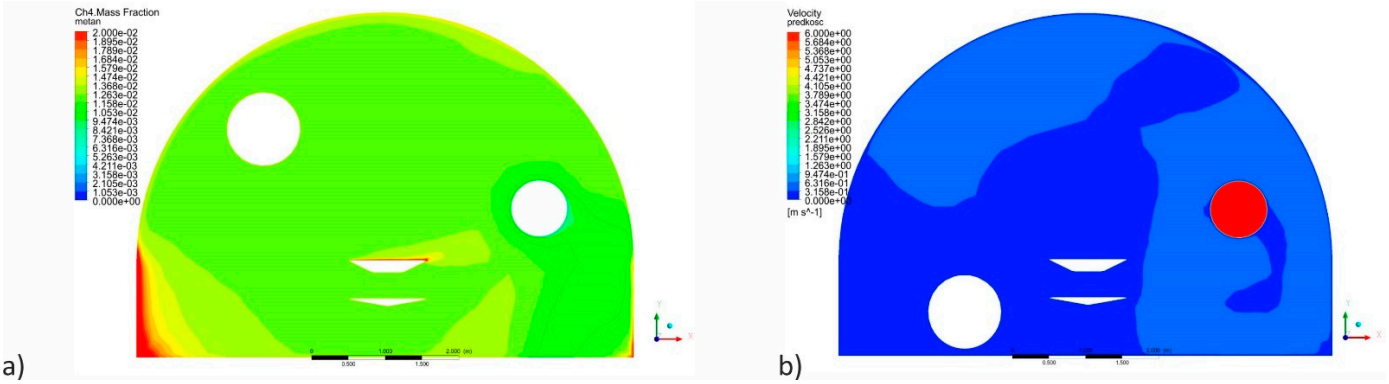

Figure 13. Cross-section of roadway at the distance of 34 m to the face for the case L_o = 15 m, (**a**) methane concentration field, (**b**) air velocity field.

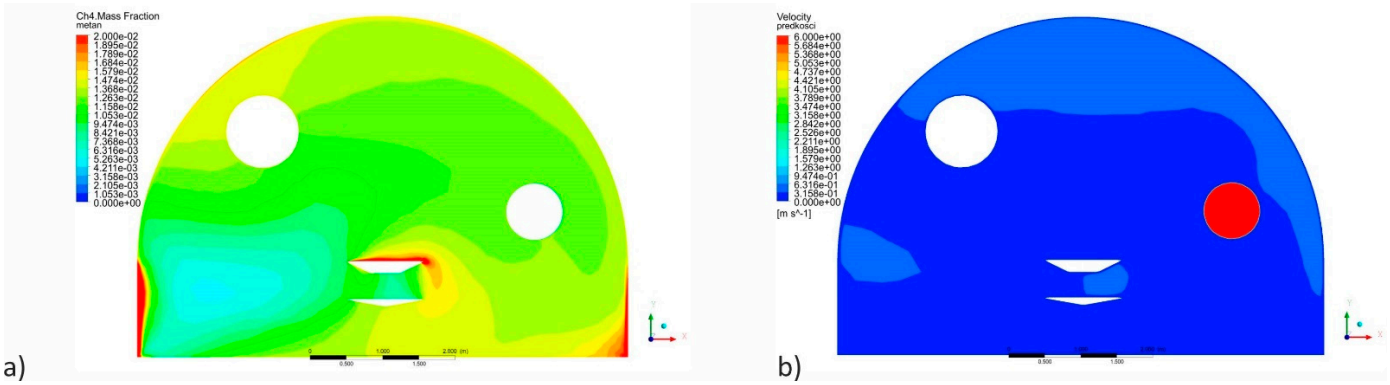

Figure 14. Cross-section of roadway at the distance of 39 m to the face for the case L_o = 20 m, (**a**) methane concentration field, (**b**) air velocity field.

To sum up, it should be stated that, until now, a belief has been held that methane concentrations in an overlap zone result from only a small amount of air flowing through this zone with a swirling motion. The results of numerical simulations have shown that the air-methane mixture flowing out of the scrubber returns to the overlap zone. Therefore, there might be an additional reason for an increase in the methane concentration in that zone. If the length of the overlap zone is short (in the case of L_o = 5 m), the velocity profile of the swirling air, leaving the WFAD, may be disturbed. It may disturb the swirl of fresh air and increase methane concentration under the roof of the overlap zone. In turn, in cases of L_o = 15 m and L_o = 20 m, the backflow zone in the behind-face zone is lengthened, where methane concentration may increase compared to the case of L_o = 10 m. However, in the behind-face zone, methane concentration is the lowest in all the cases. In the case of increasing the overlap zone's length, the distance in which the concentration equalization occurs moves further from the face (Figure 15). The advance rate of the heading face is practically in proportion to the increase in the length of the overlap zone. The mean methane concentrations in the analyzed cross-sections indicate that extending the overlap zone would be beneficial because it would increase the region with the reduced methane concentration. However, methane concentrations in the behind-face zone are higher.

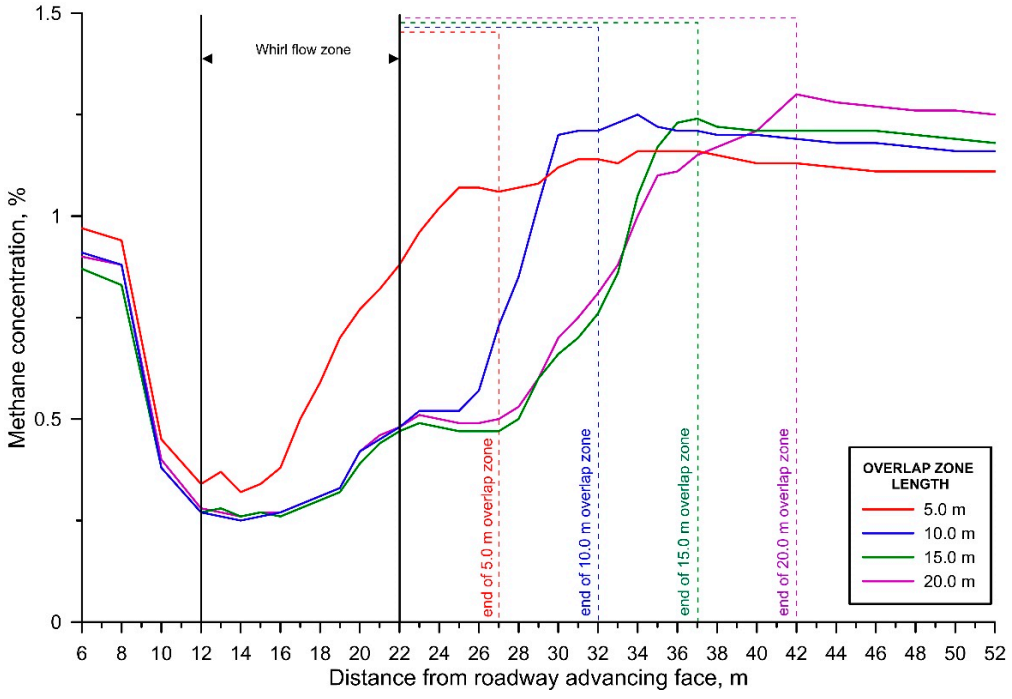

Figure 15. Mean methane concentration within the roadway in function of the distance to the face.

Therefore, the methane concentration was analyzed at 11 characteristic points of the cross-section within the length of the roadway (Figure 16). The locations of the analyzed places in the cross-section are shown in Figure 16. Results show the lowest concentration of methane for case L_o = 10 m at most points of the cross-section; therefore, it should be assumed that the best case is L_o = 10 m. Figure 17a,k shows methane concentration at measurement points within the roadway.

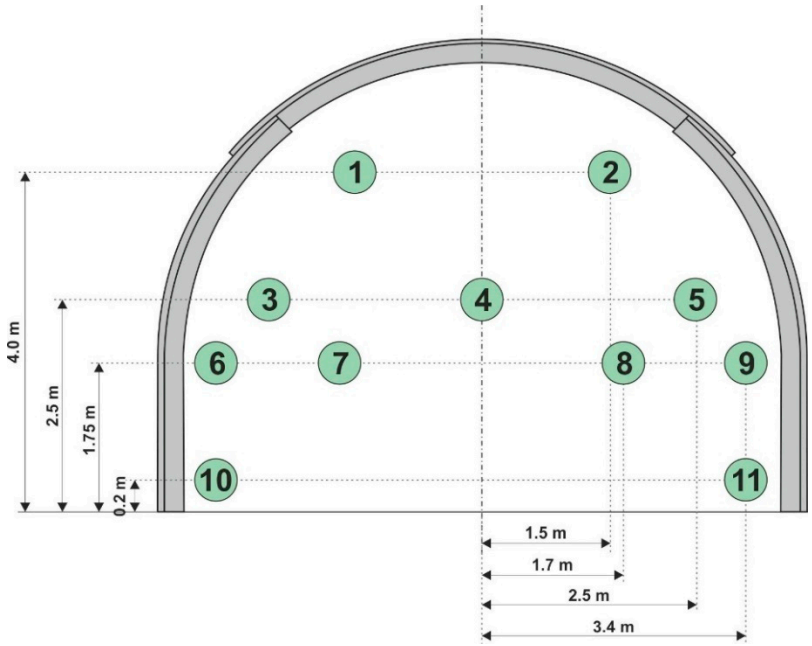

Figure 16. Location of measurement points in the cross-section for the analysis of methane concentration within the roadway.

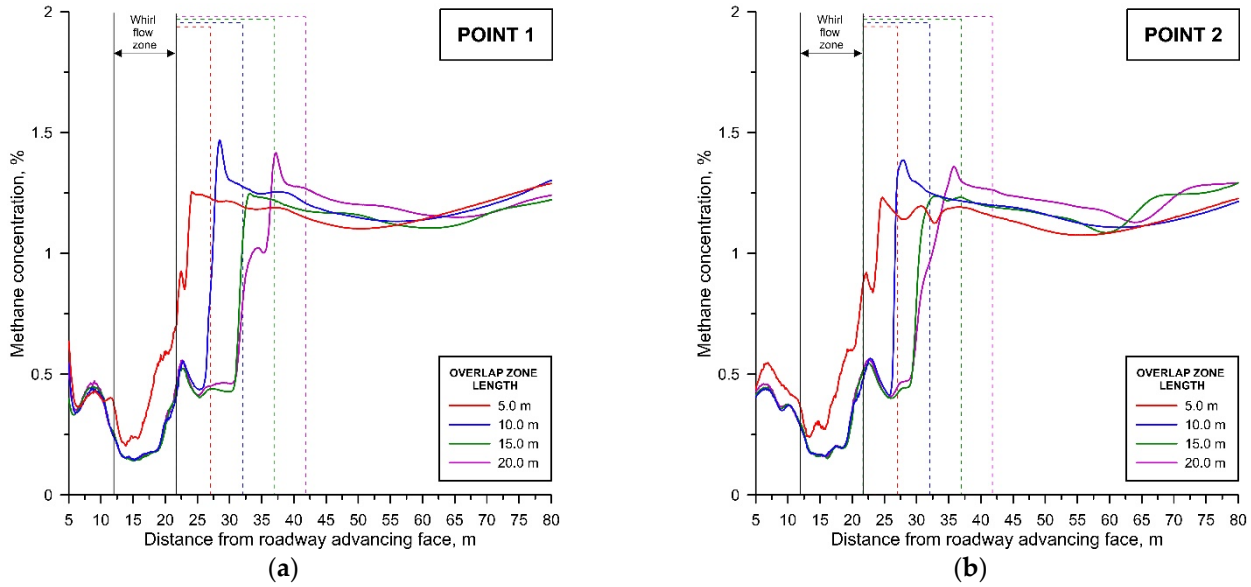

Figure 17. *Cont.*

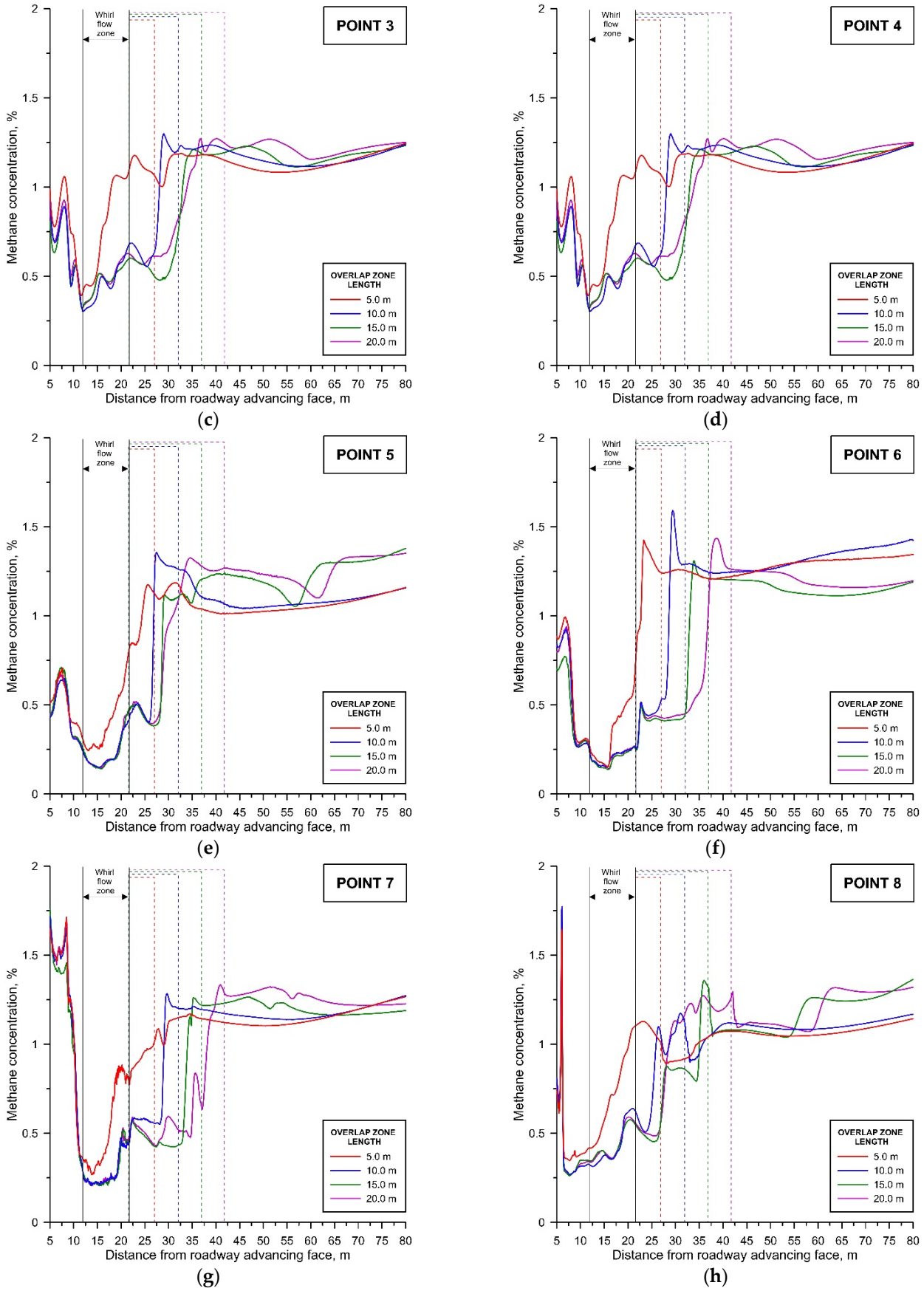

Figure 17. *Cont.*

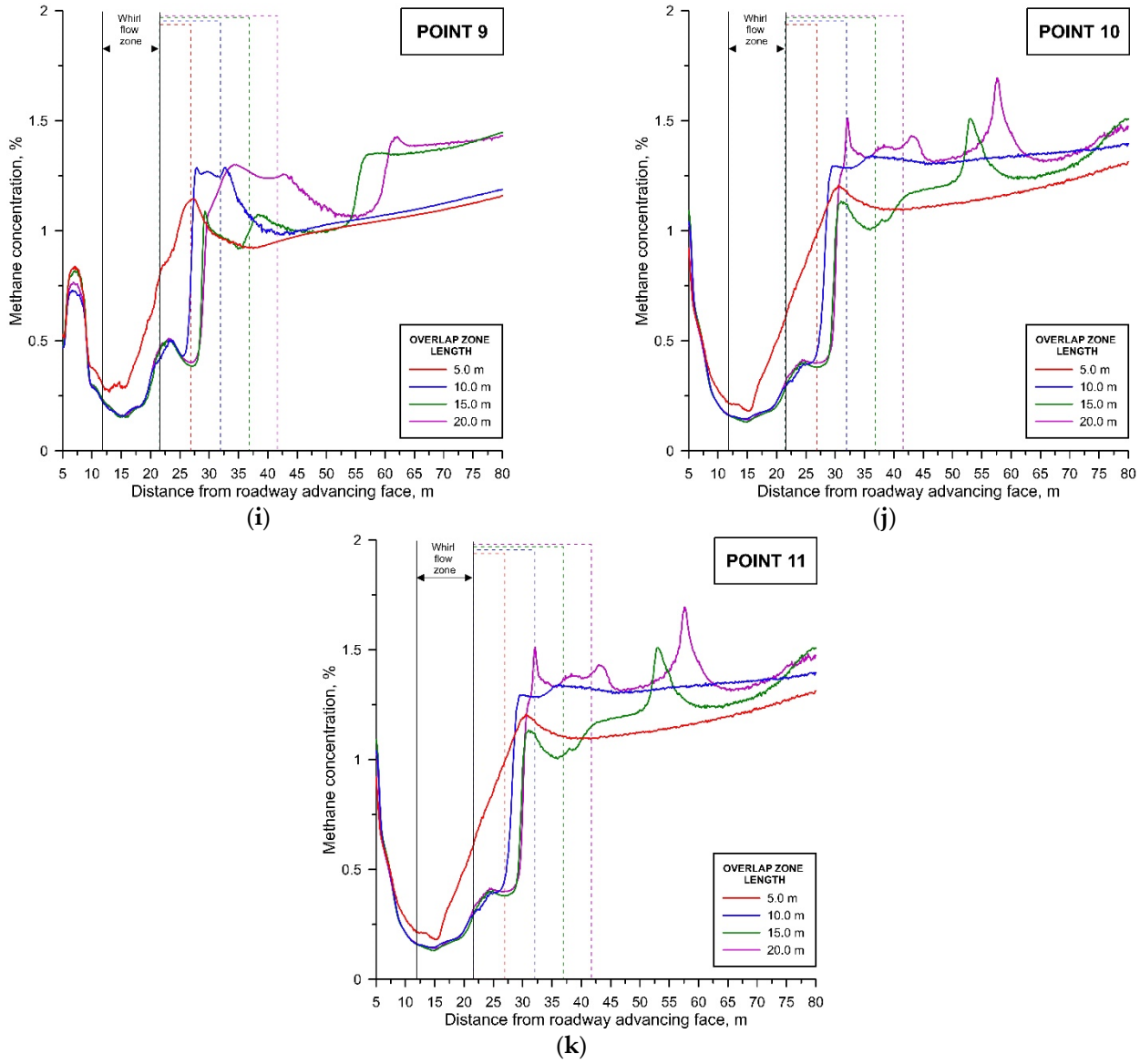

Figure 17. Methane concentration at measurement points within the roadway, acc. to Figure 16, (**a**) point 1; (**b**) point 2; (**c**) point 3; (**d**) point 4; (**e**) point 5; (**f**) point 6; (**g**) point 7; (**h**) point 8; (**i**) point 9; (**j**) point 10; (**k**) point 11.

The authors realize that they obtained the results for specific dimensions of the excavation and its equipment. Nevertheless, the detected backflows in the behind-face zone will always limit the swirling flow of intake air in the overlap zone. The qualitative effect of this phenomenon may be different in other roadways. However, the computational fluid dynamics (CFD) approach can be used to study this phenomenon. However, there is no doubt that a minor impact of return air backflows will occur if the length of the ducts' overlap zones range from 5 to 10 m.

6. Conclusions

The selection of an auxiliary ventilation system for development workings predicted for the conditions of methane emission should consider the methane distribution along the advancing roadway equipped with ventilation and technological devices. The release of methane and its distribution with the air in a run-of-mine roadway was simulated using the computational fluid dynamics (CFD) approach for primary forcing with an exhaust overlap system. Investigation into the length of the overlap zone between the force and exhaust ducts under the conditions of methane emission were shown:

1. When considering the distribution of methane concentrations in roadways with auxiliary ventilation, it is essential to properly reflect the geometry and equipment of the roadway and the number, location, and efficiency of methane emission sources. The roadway ventilation model, validated by measurements, confirmed the validity of the assumed functions of changes in methane emission from three sources: coal surface in the face, coal surfaces in the sidewalls of the roadway, and mined coal transported by a conveyor.

2. The whirl-flow air duct (WFAD) at the end of the force duct ensures swirling airflow both to the face and in the overlap zone. The supply of 20% more air through the forcing duct than the air discharged through a short exhaust duct ensures effective mixing of gases with a swirling motion and the removal of methane concentration from under the roof of the roadway.

3. The length of the overlap zone is essential to the distribution of methane concentration in the roadway. The simulation cases carried out for all four lengths of 5 m, 10 m, 15 m and 20 m of the overlap zone showed that methane concentrations in that zone are effectively lowered. However, the results obtained have also shown an air backflow along the sidewall opposite the exhaust overlap duct. It is due to the formation of a negative pressure zone around the free stream, leaving the exhaust overlap duct, in which the air backflow phenomenon occurs.

4. If the length of the overlap zone is only 5 m, the return air backflow may disturb the stabilized velocity profile of the intake air, leaving the WFAD. If the overlap zone is 15 m or 20 m, the range of the air backflow is greater and results in higher methane concentrations in the region from the scrubber outlet to the point of free stream die down.

5. The test results have shown that an overlap distance ranging from 5 to 10 m should be maintained between the force and the exhaust ducts for methane control in a face zone. The roadway driving organization should consider the necessity of simultaneous reconstruction of a forcing duct ended with the WFAD and an exhaust duct equipped with a scrubber.

Author Contributions: Conceptualization, D.O.; methodology, D.O.; software, P.D.; validation, P.D.; formal analysis, M.K.; investigation, D.O., M.K. and P.D.; resources, M.K. and P.D.; data curation, M.K.; writing—original draft preparation, D.O.; writing—review and editing, M.K.; visualization, M.K. and P.D.; supervision, D.O.; project administration, D.O. All authors have read and agreed to the published version of the manuscript.

Funding: The article was prepared as part of the Subsidy for the Maintenance and Development of Research Potential at Faculty of Civil Engineering and Resource Management AGH University of Science and Technology No. 16.16.100.215.

Institutional Review Board Statement: Not applicable.

Informed Consent Statement: Informed consent was obtained from all subjects involved in the study.

Data Availability Statement: Upon authors' request.

Acknowledgments: The authors would like to thank the mine personnel for their inputs and assistance.

Conflicts of Interest: The authors declare no conflict of interest.

References

1. Toraño, J.; Torno, S.; Menendez, M.; Gent, M.; Velasco, J. Models of methane behaviour in auxiliary ventilation of underground coal mining. *Int. J. Coal Geol.* **2009**, *80*, 35–43. [CrossRef]
2. Fang, Y.; Yao, Z.; Lei, S. Air flow and gas dispersion in the forced ventilation of a road tunnel during construction. *Undergr. Space* **2019**, *4*, 168–179. [CrossRef]
3. Rahimi, S.; Ataee-Pour, M.; Madani, H.; Aminossadati, S.M. Investigating the impact of gas emission uncertainty on airflow distribution in an auxiliary ventilation system using CFD and Monte-Carlo simulation. *Build. Environ.* **2021**, *204*, 108165. [CrossRef]

4. Moloney, K.W.; Lowndes, I.S.; Hargrave, G.K. Analysis of flow patterns in drivages with auxiliary ventilation. *Trans. Inst. Min. Metall. Sect. A Min. Ind.* **1999**, *108*, 17–26.
5. Lowndes, S.; Crossley, A.J.; Yang, Z.Y. The ventilation and climate modeling of rapid development tunnel drainages. *Tunn. Undergr. Space Technol.* **2004**, *19*, 139–150. [CrossRef]
6. Hua, Y.; Nie, W.; Wei, W.; Liu, Q.; Liu, Y.; Peng, H. Research on multi-radial swirling flow for optimal control of dust dispersion and pollution at a fully mechanized tunnelling face. *Tunn. Undergr. Space Technol.* **2018**, *79*, 293–303. [CrossRef]
7. Hua, Y.; Nie, W.; Liu, Q.; Peng, H.; Wei, W.; Cai, P. The development and application of a novel multi-radial-vortex-based ventilation system for dust removal in a fully mechanized tunnelling face. *Tunn. Undergr. Space Technol.* **2020**, *98*, 103253. [CrossRef]
8. Ren, T.; Wang, Z.; Coope, G. CFD modelling of ventilation and dust flow behaviour above an underground bin and the design of an innovative dust mitigation system. *Tunn. Undergr. Space Technol.* **2014**, *41*, 241–254. [CrossRef]
9. Shi, G.; Liu, M.; Guo, Z.; Hu, F.; Wang, D. Unsteady simulation for optimal arrangement of dedusting airduct in coal mine heading face. *J. Loss Prev. Process Ind.* **2017**, *46*, 45–53. [CrossRef]
10. Cao, Z.; Liu, X. Study on the Characteristics of Flow Field and Gas Migration in Gas Tunnels. *IOP Conf. Ser. Mater. Sci. Eng.* **2020**, *741*, 012039. [CrossRef]
11. Torno, S.; Toraño, J.; Ulecia, M.; Allende, C. Conventional and numerical models of blasting gas behaviour in auxiliary ventilation of mining headings. *Tunn. Undergr. Space Technol.* **2013**, *34*, 73–81. [CrossRef]
12. Wala, A.; Jacob, J.; Brown, J.; Huang, G. New approaches to mine-face ventilation. *Min. Eng.* **2003**, *55*, 25–30.
13. Wala, A.M.; Vytla, S.; Taylor, C.D.; Huang, G. Mine face ventilation: A comparison of CFD results against benchmark experiments for the CFD code validation. *Min. Eng.* **2007**, *59*, 49–55.
14. Petrov, T.; Wala, A.M.; Huang, G. Parametric study of airflow separation phenomenon at face area during deep cut continuous mining. *Min. Technol.* **2013**, *122*, 208–214. [CrossRef]
15. Nakayama, S.; Ichinose, M.; Uchino, K.; Inoue, M. Scale Tests, In-situ Measurements and Simulation of Methane Gas Distribution at Heading Faces. In Proceedings of the 8th US Mine Ventilation Symposium, Rolla, MO, USA, 11–17 June 1999; pp. 85–90.
16. Gong, X.-Y.; Jiao, W.-Y.; Wei, Y.-S.; Xue, H. Flow Field Characteristic Analysis for Auxiliary Ventilation during Different Excavation Stages in Coal Mine. In Proceedings of the 2016 International Conference on Energy Development and Environmental Protection (EDEP 2016), Beijing, China, 11–12 June 2016; ISBN 978-1-60595-360-1. [CrossRef]
17. Daloğlu, G.; Önder, M.; Parra, T. Modeling of Methane and Air Velocity Behavior in an Auxiliary Ventilated Coal Heading. *Arch. Min. Sci.* **2021**, *66*, 69–84. [CrossRef]
18. Kurnia, J.C.; Sasmito, A.P.; Mujumdar, A.S. Simulation of a novel intermittent ventilation system for underground mines. *Tunn. Undergr. Space Technol.* **2014**, *42*, 206–215. [CrossRef]
19. Sasmito, A.P.; Birgersson, E.; Ly, H.C.; Mujumdar, A.S. Some approaches to improve ventilation system in underground coal mines environment—A computational fluid dynamic study. *Tunn. Undergr. Space Technol.* **2013**, *34*, 82–95. [CrossRef]
20. Hasheminasaba, F.; Bagherpoura, R.; Aminossadatib, S.M. Numerical simulation of methane distribution in development zones of underground coal mines equipped with auxiliary ventilation. *Tunn. Undergr. Space Technol.* **2019**, *89*, 68–77. [CrossRef]
21. Pawiński, J.; Roszkowski, J. Emission of methane into mine galleries driven in coal by means of combined cutter-loaders. *Arch. Min.* **1985**, *30*, 207–213.
22. Szlązak, N.; Tor, A. Distribution of methane in mining galleries excavated with continuous miners with regard to air leakages. *Arch. Min. Sci.* **1997**, *42*, 477–496.
23. Roszkowski, J.; Pawiński, J.; Nowak, B. Stężenie metanu wydzielającego się w przodku wyrobiska chodnikowego z węgla urabianego kombajnem. *Arch. Min.* **1994**, *39*, 463–471.
24. Pawiński, J. Flows with mass and momentum exchange in some issues of mine ventilation. *AGH Univ. Sci. Technol. J. Min.* **1971**, *34*, 2–63.
25. Tutak, M. The Influence of the Permeability of the Fractures Zone Around the Heading on the Concentration and Distribution of Methane. *Sustainability* **2020**, *12*, 16. [CrossRef]
26. Szlązak, N.; Borowski, M.; Obracaj, D.; Swolkień, J.; Korzec, M. *Odmetanowanie Górotworu w Kopalniach Węgla Kamiennego (Methane Drainage in Coal Mines)*; AGH University of Science and Technology Press: Krakow, Poland, 2015.
27. Fluent, A. *User's Guide. Fluent 2020 R2*; ANSYS, Inc.: Canonsburg, PA, USA, 2020.
28. Li, Z.; Liu, H.; Xu, Y.; Li, R.; Jia, M.; Zhang, M. Numerical Analysis on the Thermal Performance in an Excavating Roadway with Auxiliary Ventilation System. *Int. J. Environ. Res. Public Health* **2021**, *18*, 1184. [CrossRef] [PubMed]
29. Wang, W.; Zhang, C.; Yang, W.; Xu, H.; Li, S.; Li, C.; Ma, H.; Qi, G. In Situ Measurements and CFD Numerical Simulations of Thermal Environment in Blind Headings of Underground Mines. *Processes* **2019**, *7*, 313. [CrossRef]
30. Zhou, B.; Chang, P.; Xu, G. Computational Fluid Dynamic Simulation of Inhaled Radon Dilution by Auxiliary Ventilation in a Stone-Coal Mine Laneway and Dosage Assessment of Miners. *Processes* **2019**, *7*, 515. [CrossRef]